

Measuring the phonon-assisted spectral function by using a non-equilibrium three-terminal single-molecular device

Juntao Song¹, Qing-feng Sun^{1,*}, Jinhua Gao^{1,2}, and X.C. Xie^{1,2}

¹*Beijing National Lab for Condensed Matter Physics and Institute of Physics,
Chinese Academy of Sciences, Beijing 100080, China*

²*Department of Physics, Oklahoma State University, Stillwater Oklahoma, 74078 USA*
(Dated: February 9, 2022)

The electron transport through a three-terminal single-molecular transistor (SMT) is theoretically studied. We find that the differential conductance of the third and weakly coupled terminal versus its voltage matches well with the spectral function versus the energy when certain conditions are met. Particularly, this excellent matching is maintained even for complicated structure of the phonon-assisted side peaks. Thus, this device offers an experimental approach to explore the shape of the phonon-assisted spectral function in detail. In addition we discuss the conditions of a perfect matching. The results show that at low temperatures the matching survives regardless of the bias and the energy levels of the SMT. However, at high temperatures, the matching is destroyed.

PACS numbers: 73.63.Kv, 71.38.-k, 85.65.+h

I. INTRODUCTION

In the past decade, transport properties of single-molecule transistors (SMT) have attracted great attention due to the potential application for the new generation of electron devices. Because of the intrinsic vibrational freedom in molecules, the molecular electronic transistor also provides a new opportunity for exploring the vibration-electronic (i.e. electron-phonon) interactions at single molecule level. The electron-phonon interaction in a SMT leads to some interesting effects, such as phonon-assisted tunneling, the red shift of SMT energy levels, and generation of the thermal energy. Such features are interesting and have been extensively investigated both experimentally and theoretically in recent years. Park *et al.*¹ experimentally studied the current-bias (I-V) characteristic of an individual C₆₀ molecule connected to gold electrodes and have observed the obvious phonon-assisted tunneling sub-steps in the I-V curves. Later the current of a suspended individual single-wall nanotube device is measured and two phonon-assisted sub-peaks on the two sides of the main resonant peak are clearly visible in the differential conductance versus the gate voltage, which is due to the radial breathing phonon mode.^{2,3} Very recently, also in the device of a suspended single-wall nanotube but with much lower temperatures, the higher order phonon-assisted sub-steps on the I-V curves have been experimentally demonstrated by Sapmaz *et al.*⁴

On the theoretical side, there have also been a large amount of studies on the quantum transport behavior of a SMT or a quantum dot (QD) coupled to local phonon modes.^{5,6,7,8,9,10,11} About 15 years ago, Wingreen *et al.* studied the electron transport through a QD coupled to the phonon modes by combining the scattering theory and the Green's function method, and the phonon-induced transmission sidebands were found.⁵ Using the real-time renormalization-group method, Keil *et al.*⁶ have investigated the quantum transport phenomena through cou-

pled QDs with a phonon bath, and a solution for stationary current is obtained. In addition, the shot-noise spectroscopy of the current of a SMT having a local phonon mode is reported by Zhu and Balatsky.⁸ Since the current, the conductance, the shot-noise, *etc.*, are all closely related to the local electronic spectral functions $A(\omega)$, the spectral function has also been extensively studied. The spectral function is found to be strongly dependent on the positions of the SMT (or QD) energy levels and the tunneling strengths Γ between the leads and the SMT (or QD).⁹ On the other hand, by using a different approximation, Chen *et al.* also investigated the spectral function and the current through a SMT,¹⁰ and the spectral function in their results exhibits intriguing features. At low temperatures and under the condition that the energy level is near the Fermi surface, the side peaks in the spectral function are clearly non-Lorentzian in shape. The side peaks on one side changes gradually while the other side change abruptly with changing of energy. These are quite different comparing with the previous results. Due to the importance of the spectral function $A(\omega)$ as well as that the spectral function of a SMT coupled to a phonon mode is not well understood (i.e. the results of $A(\omega)$ are qualitatively different for using different approximations), thus it is quite beneficial to design an experimental set-up to directly measure the spectral function of a SMT.

Recently, some studies have investigated the Kondo effect in QDs coupled to the three terminals, in which the third terminal acts as an exploring tip to measure the Kondo peaks in the spectral function.^{12,13} Can the intriguing characteristics of the phonon-assisted side peaks in the spectral function also be explored in a three-terminal set-up? It is the purpose of this work to theoretically analyze the feasibility of this scheme. We consider the system of either SMT or QD coupled to three leads and a local phonon mode. Here the third lead is introduced as an exploring tip. We find that the spectral function quite often matches the differential conductance

of the third lead. If the third lead is weakly coupled and the temperature T is low ($k_B T \ll \hbar \omega_0$ with ω_0 being the phonon frequency), this matching is almost perfect (including the abrupt changes associated with the phonon-assisted side peaks), so the spectral function, in particular the phonon-assisted side peaks, can be directly detected using the differential conductance. On the other hand, if the coupling of the third lead is large but still at low temperature, the matching is in qualitative agreement. However, at high temperature, the matching is destroyed even for weakly-coupled third lead.

The rest of this paper is organized as follows. We introduce the model in Sec. II and derive formulas of the spectral function and the differential conductance in Sec. III. In Sec. IV, we show the numerical results and present discussions of those results. Finally, a brief summary is given in Sec. V.

II. MODEL HAMILTONIAN

The device under our consideration is illustrated in Fig.1. It consists of a SMT or QD connected to three metallic leads. An electron in the SMT is also coupled to a single phonon mode. Due to the big energy gap between two quantum levels in the SMT, only one relevant quantum level is considered. The Hamiltonian of the device is written as:

$$H = H_{Leads} + H_{ph} + H_D + H_T. \quad (1)$$

The first two terms are, respectively, the Hamiltonian for electrons in the three leads and the Hamiltonian for the phonon part,

$$H_{Leads} = \sum_{\alpha,k} \varepsilon_{\alpha k} c_{\alpha k}^\dagger c_{\alpha k}, \quad (2)$$

$$H_{ph} = \omega_0 b^\dagger b. \quad (3)$$

Here $\alpha = L, R$, and 3 respectively represent the left, the right, and the third leads, and $c_{\alpha k}^\dagger (c_{\alpha k})$ creates (annihilates) an electron with the energy $\varepsilon_{\alpha k}$ in the lead α . Analogously, $b^\dagger (b)$ is the phonon creation (annihilation) operator and ω_0 is the vibrational frequency of the phonon. The third term in Eq.(1) is

$$H_D = [\varepsilon_0 + \lambda(b^\dagger + b)]d^\dagger d, \quad (4)$$

where $d^\dagger (d)$ is the electron creation (annihilation) operator in the SMT with the energy level ε_0 , and λ describes the coupling strength between the SMT and the local phonon mode. The last term in Eq.(1) describes the tunnelling coupling between the SMT and the three leads,

$$H_T = \sum_{\alpha,k} [V_{\alpha k} c_{\alpha k}^\dagger d + H.c]. \quad (5)$$

It is often useful to take a canonical transformation with:^{10,14} $\bar{H} = e^s H e^{-s}$ and $s = (\lambda/\omega_0)(b^\dagger - b)d^\dagger d$. Under

this canonical transformation the Hamiltonian (1) varies into

$$\bar{H} = \bar{H}_{el} + \bar{H}_{ph}, \quad (6)$$

where

$$\bar{H}_{el} = \sum_{\alpha,k} \varepsilon_{\alpha k} c_{\alpha k}^\dagger c_{\alpha k} + \bar{\varepsilon}_0 d^\dagger d + \sum_{\alpha,k} [\bar{V}_{\alpha k} c_{\alpha k}^\dagger d + H.c], \quad (7)$$

and

$$\bar{H}_{ph} = \omega_0 b^\dagger b. \quad (8)$$

Obviously, due to the electron-phonon interaction, the energy level ε_0 of the SMT is renormalized to $\bar{\varepsilon}_0 = \varepsilon_0 - g\omega_0$ with $g = (\lambda/\omega_0)^2$, and the tunnelling matrix element V_k is varied into $\bar{V}_k = V_k X$ where $X = \exp[-(\lambda/\omega_0)(b^\dagger + b)]$. Up till now, no approximation has been made, the Hamiltonian (6) is completely equivalent to the Hamiltonian (1).¹⁴

III. THE SPECTRAL FUNCTION AND THE DIFFERENTIAL CONDUCTANCE

In this section, we calculate the spectral function $A(\omega)$ of the SMT and the differential conductance of the third lead. From the results by Meir and Wingreen, the spectral function $A(\omega)$ and the current can be represented by the Green functions of the SMT as:^{15,16}

$$A(\omega) = i[G^>(\omega) - G^<(\omega)] = i[G^r(\omega) - G^a(\omega)]. \quad (9)$$

$$J_\alpha = \frac{e}{\hbar} \int \frac{d\omega}{2\pi} Tr\{ \Gamma_\alpha [iG^<(\omega) + A(\omega)f_\alpha(\omega)] \}. \quad (10)$$

Here $f_\alpha(\omega) = 1/\{\exp[(\omega - \mu_\alpha)/k_B T] + 1\}$ is the Fermi distribution function with the chemical potential μ_α , $\Gamma_\alpha(\omega) = 2\pi \sum_k |V_{\alpha k}|^2 \delta(\varepsilon_{\alpha k} - \omega)$ describes the coupling strength between the lead α and the SMT, and $G^{<,>,r,a}$ are the standard lesser, greater, retarded, advanced Green functions.^{16,17} Because of the existence of the electron-phonon interaction, it is difficult to directly solve these Green functions from the equation of motion technique or the Dyson equations. As it is done in some previous papers,¹⁰ here we take the same approximation to replace the operator X and X^\dagger in Hamiltonian (6) with their expectation value $\langle X \rangle = \langle X^\dagger \rangle = \exp[-g(N_{ph} + 1/2)]$, where $N_{ph} = 1/[\exp(\beta\omega_0) - 1]$ is the phonon population.¹⁸ This approximation is valid when the tunneling strengths Γ_α are smaller than the electron-phonon interaction, i.e, $\Gamma_\alpha \ll \lambda$. After this approximation, the Hamiltonian (6) is decoupled into two independent parts, electronic part and phonon part. Next, we also need to decouple the Green functions. In many previous papers,⁸ they decouple the retarded (advanced) Green functions $G^{r,a}$ directly. However, such decoupling has some defects as pointed out in a recent work by Chen

*et al.*¹⁰ Here we employ the decoupling method in the Ref.⁽¹⁰⁾, to directly decouple the lesser and greater Green functions $G^{<,>}$ instead of the retarded and advanced Green functions $G^{r,a}$. After the decoupling, the lesser and greater Green functions $G^{<,>}$ are:

$$G^{<}(t, t') = \bar{G}^{<}(t, t') e^{-\Phi(t'-t)}, \quad (11)$$

$$G^{>}(t, t') = \bar{G}^{>}(t, t') e^{-\Phi(t-t')}, \quad (12)$$

where $\bar{G}^{<,>}(t, t')$ are the Green functions of the Hamiltonian \bar{H}_{el} , and $\Phi(t)$ is

$$\Phi(t) = g [N_{ph}(1 - e^{i\omega_0 t}) + (N_{ph} + 1)(1 - e^{-i\omega_0 t})]. \quad (13)$$

Using the identity¹⁴ $e^{z \cos \theta} = \sum_{n=-\infty}^{+\infty} I_n(z) e^{in\theta}$, the greater and lesser Green functions can be expanded as

$$G^{<}(\omega) = \sum_{n=-\infty}^{+\infty} B_n \bar{G}^{<}(\omega + n\omega_0), \quad (14)$$

$$G^{>}(\omega) = \sum_{n=-\infty}^{+\infty} B_n \bar{G}^{>}(\omega - n\omega_0), \quad (15)$$

where the coefficients $B_n = e^{-g(2N_{ph}+1)} e^{n\omega_0/2k_B T} I_n(2g\sqrt{N_{ph}(N_{ph}+1)})$ and $I_n(z)$ is the n th Bessel function of complex argument. Thus we can rewrite the spectral function $A(\omega)$ as

$$\begin{aligned} A(\omega) &= i[G^{>}(\omega) - G^{<}(\omega)] \\ &= \sum_{n=-\infty}^{+\infty} iB_n [\bar{G}^{>}(\omega - n\omega_0) - \bar{G}^{<}(\omega + n\omega_0)] \end{aligned} \quad (16)$$

Following the standard derivation,^{14,16,17} the self-energies $\bar{\Sigma}$ of the coupling to the leads for the Hamiltonian \bar{H}_{el} can be easily obtained as:

$$\bar{\Sigma}^{r(a)}(\omega) = \sum_{\alpha,k} |\bar{V}_{\alpha k}|^2 g_{\alpha k}^{r(a)}(\omega) = \sum_{\alpha} [\bar{\Lambda}_{\alpha}(\omega) \mp \frac{i}{2} \bar{\Gamma}_{\alpha}(\omega)] \quad (17)$$

$$\bar{\Sigma}^{<}(\omega) = \sum_{\alpha,k} |\bar{V}_{\alpha k}|^2 g_{\alpha k}^{<}(\omega) = i \sum_{\alpha} \bar{\Gamma}_{\alpha}(\omega) f_{\alpha}(\omega), \quad (18)$$

$$\bar{\Sigma}^{>}(\omega) = \sum_{\alpha,k} |\bar{V}_{\alpha k}|^2 g_{\alpha k}^{>}(\omega) = -i \sum_{\alpha} \bar{\Gamma}_{\alpha}(\omega) [1 - f_{\alpha}(\omega)] \quad (19)$$

where $\bar{\Gamma}_{\alpha} = \Gamma_{\alpha} \exp[-g(2N_{ph}+1)]$ since the tunneling elements $V_{\alpha k}$ have been amended by electron-phonon interaction. To take the wideband limit,^{16,17} i.e. to assume that Γ_{α} then $\bar{\Gamma}_{\alpha}$ are independent with the energy ω , the above self-energies reduce into:

$$\bar{\Sigma}^{r(a)} = \mp \frac{i}{2} (\bar{\Gamma}_L + \bar{\Gamma}_R + \bar{\Gamma}_3), \quad (20)$$

$$\bar{\Sigma}^{<}(\omega) = i \sum_{\alpha} \bar{\Gamma}_{\alpha} f_{\alpha}(\omega), \quad (21)$$

$$\bar{\Sigma}^{>}(\omega) = -i \sum_{\alpha} \bar{\Gamma}_{\alpha} [1 - f_{\alpha}(\omega)]. \quad (22)$$

By using these self-energies, the dressed retarded (advanced) Green function $\bar{G}^{r(a)}$, then the dressed lesser and greater Green functions $\bar{G}^{<,>}$ can be readily obtained from Dyson equations and Keldysh equations:

$$\bar{G}^{r(a)}(\omega) = [\bar{g}^{r(a)}(\omega) - \bar{\Sigma}^{r(a)}(\omega)]^{-1}, \quad (23)$$

$$\bar{G}^{<}(\omega) = \bar{G}^r(\omega) \bar{\Sigma}^{<}(\omega) \bar{G}^a(\omega) = i \bar{f}(\omega) \bar{A}(\omega), \quad (24)$$

$$\bar{G}^{>}(\omega) = \bar{G}^r(\omega) \bar{\Sigma}^{>}(\omega) \bar{G}^a(\omega) = -i [1 - \bar{f}(\omega)] \bar{A}(\omega) \quad (25)$$

where

$$\bar{A}(\omega) = \frac{\bar{\Gamma}_L + \bar{\Gamma}_R + \bar{\Gamma}_3}{(\omega - \bar{\epsilon}_0)^2 + (\bar{\Gamma}_L + \bar{\Gamma}_R + \bar{\Gamma}_3)^2/4}, \quad (26)$$

and

$$\bar{f}(\omega) = \frac{\bar{\Gamma}_L f_L(\omega) + \bar{\Gamma}_R f_R(\omega) + \bar{\Gamma}_3 f_3(\omega)}{\bar{\Gamma}_L + \bar{\Gamma}_R + \bar{\Gamma}_3}. \quad (27)$$

After solving $\bar{G}^{<,>}$, the lesser and greater Green functions $G^{<,>}(\omega)$, the electronic spectral function $A(\omega)$ of the SMT, and then the current can be calculated from the above Eqs. (9), (10), (14), and (15), straightforwardly.

At last, the differential conductance G_3 of the third terminal can be acquired by performing $G_3 = \partial J_3 / \partial V_3$

$$\begin{aligned} G_3 &= \sum_{n=-\infty}^{+\infty} \frac{e^2 \Gamma_3}{\hbar k T} B_n \int \frac{d\omega}{2\pi} \{ f_3(\omega) [1 - f_3(\omega)] \\ &\quad \times [\bar{A}(\omega_2) \bar{f}(\omega_2) + \bar{A}(\omega_1) [1 - \bar{f}(\omega_1)]] \\ &\quad - c [1 - f_3(\omega)] f_3(\omega_2) [1 - f_3(\omega_2)] \bar{A}(\omega_2) \\ &\quad - c f_3(\omega) f_3(\omega_1) [1 - f_3(\omega_1)] \bar{A}(\omega_1) \}, \end{aligned} \quad (28)$$

where $\omega_1 = \omega - n\omega_0$, $\omega_2 = \omega + n\omega_0$, and $c = \bar{\Gamma}_3 / (\bar{\Gamma}_L + \bar{\Gamma}_R + \bar{\Gamma}_3)$.

IV. NUMERICAL RESULTS AND DISCUSSIONS

In this section, we study numerically the spectral function $A(\omega)$ and the differential conductance G_3 . In the numerical calculation, the coupling strengths $\Gamma_{L/R}$ between the left/right lead and the SMT is set to be unity ($\Gamma_L = \Gamma_R \equiv \Gamma = 1$), as an energy unit. The main purpose in the present work is to study whether the curve of the spectral function $A(\omega)$ versus the energy ω can map into the curve G_3 - V_3 , i.e. whether the intriguing phonon-assisted side peaks in the spectral function $A(\omega)$ can be observed by measuring the conductance G_3 of the third lead. First, let us show the spectral function of the two-terminal SMT with $\Gamma_3 = 0$. Note that this spectral function $A(\omega)$ is the object of our study. When the SMT is coupled to the phonon mode, one main characteristic of $A(\omega)$ is the appearance of the phonon-assisted side peaks. At the zero bias case ($\mu_L = \mu_R = 0$) and the renormalized level $\bar{\epsilon}_0 = 0$, the side peaks are non-Lorentzian in shape, in

which one side of the side peaks still looks like the Lorentzian form but the other side drops abruptly (see Fig.2). When $\bar{\varepsilon}_0$ (i.e. $|\bar{\varepsilon}_0|/\Gamma \gg 0$) is far away from the chemical potentials μ_L, μ_R , the side peaks are asymmetry on the two sides of the main peak, and the side peaks disappear on one side. Furthermore, with a non-zero bias V ($V = \mu_L - \mu_R$) or raising temperature T , these phonon-assisted side peaks exhibit more complex profiles. These characteristics of the spectral function $A(\omega)$ have been found in a previous study.¹⁰ Our goal here is to propose a scheme to measure the spectral function $A(\omega)$ by using an extra third lead.

We first study the zero bias case ($\mu_L = \mu_R = 0$) with a weakly-coupled third lead ($\Gamma_3 = 0.01$). Fig.2 shows the differential conductance G_3 versus the voltage V_3 of the third lead for different renormalized level $\bar{\varepsilon}_0$. For comparison, the spectral function $A(\omega)$ versus the energy ω for the two-terminal SMT device with $\Gamma_3 = 0$ is also shown in Fig.2. When $\bar{\varepsilon}_0 = 0$. Besides the main resonant tunneling peak, some extra phonon-assisted side peaks emerge in the curve G_3-V_3 . The main peak is Lorentzian, but the side peaks exhibit non-Lorentzian characteristic. On the one side of the side peaks, the conductance G_3 falls abruptly from top to valley. In particular, we find that the curve of the conductance G_3 versus V_3 is in an excellent agreement with the curve of the spectral function $A(\omega)$ versus the energy ω . Not only are their side peaks located at the same positions, but also they have the same profiles. Even the abrupt drops overlap perfectly. Thus, in this case by measuring the differential conductance G_3 , one obtains all information on the spectral function $A(\omega)$. Increasing $\bar{\varepsilon}_0$ to 1, the side peaks in the curve of G_3-V_3 are distributed asymmetrically on two sides of the main resonant peak. The right side peak is higher than the corresponding left side peak as shown in Fig.2. However the curve of G_3-V_3 is still in an excellent matching with the spectral functions $A(\omega)$ versus ω , even the complex structure of the first right side peak (about at $V_3 = 6$) matches quite well. When $\bar{\varepsilon}_0$ is furthermore enhanced from 1 to 3, all side peaks are on the right of the main peak and all peaks are Lorentzian. Similarly the excellent agreement between the differential conductance and the spectral function are still maintained. Combining above results we find that at the zero bias case, the curve G_3-V_3 is in excellent agreement with the curve $A(\omega)-\omega$ regardless of the value of the level $\bar{\varepsilon}_0$ (i.e. ε_0). The reason lies in the fact that for the weakly-coupled lead, the transmission probability of the incoming electron with energy ω is mainly determined by the local spectral function $A(\omega)$.

Next, we study the case with a finite bias V ($V = \mu_L - \mu_R$). Fig.3 shows the differential conductance G_3 and the spectral function $A(\omega)$ for $\mu_L = -\mu_R = 3$. In the finite bias $V = 6$ and the renormalized level $\bar{\varepsilon}_0 = 0$, the phonon-assisted side peaks in the conductance G_3 are symmetrically distributed on two sides of the main resonant peak, and the form of the side peaks are Lorentzian which is in contrast to zero bias case with non-Lorentzian

side peaks (see Fig.2). However, the characteristics of the spectral function are still reflected perfectly by the differential conductance, although the spectral functions for the zero bias and the non-zero bias have a large difference. When $\bar{\varepsilon}_0$ is reduced to -3 , the left phonon-assisted side peak is obviously higher than the corresponding right side peak, the first left side peak becomes sharp, and the non-Lorentzian characteristic emerges again in the first right side peak. Although the spectral function $A(\omega)$ is so complex now, the curve of G_3-V_3 closely follows that of the spectral function, including the detail structure. With decreasing $\bar{\varepsilon}_0$ further, e.g. $\bar{\varepsilon}_0 = -6$, the conductance G_3 has a large change. In the present case, the side peaks of the right hand disappear completely and the side peaks only exit on the left hand of the main peak. We find that the curve G_3-V_3 completely matches the curve $A(\omega)-\omega$. In fact, for any bias V and any level $\bar{\varepsilon}_0$ (i.e. ε_0), the curves G_3-V_3 and $A(\omega)-\omega$ overlap perfectly regardless of complexity of the curve $A(\omega)-\omega$. This means that by measuring the differential conductance G_3 of the third lead, the spectral function $A(\omega)$, including the intriguing characteristics due to coupled to the phonon mode, can be directly observed.

In the above numerical investigation, the coupling Γ_3 between the SMT and the third lead is set to be rather weak ($\Gamma_3 = 0.01$), and the temperature T is kept at very low ($k_B T = 0.02$). For a strongly-coupled third lead and at high temperature, will the excellent agreement between the differential conductance G_3 and the spectral function $A(\omega)$ still survive? In this paragraph, we study the effect of the coupling strength Γ_3 . The temperature effect is addressed in the next paragraph. Fig.4(a) and (b) show the conductance G_3 and the spectral function $A(\omega)$ for different coupling strength Γ_3 . With increasing Γ_3 , the level in the SMT is widen, and the conductance G_3/G_0 [$G_0 = (2e^2/\hbar)(\Gamma_3/\Gamma)$] is overall reduced. To make a better comparison of the two curves G_3-V_3 and $A(\omega)-\omega$, we replace the conductance unit G_0 by an integral weighting factor G'_0 and Fig.4 (c) and (d) show G_3/G'_0 versus V_3 , here G'_0 is determined by the equation $\int \frac{dV_3}{2\pi} \frac{G_3}{G'_0} = \int \frac{d\omega}{2\pi} \frac{A(\omega)}{A_0}$. The results are as following: (i) When the third lead is weakly-coupled with a small Γ_3 ($\Gamma_3 = 0.01$), the differential conductance G_3 and the spectral function $A(\omega)$ map into each other perfectly, as discussed before. (ii) With increasing coupling strength Γ_3 , the differential conductance deviates from the spectral function gradually. When Γ_3 is in the same order of Γ (e.g. $\Gamma_3 = 0.4$ or 1), the peak of the conductance G_3 becomes lower and wider than that of the spectral function (see Fig.4). But overall the conductance G_3 still shows the similar profile of the spectral function, including the abrupt drop on the phonon-assisted side peak. In other words, the curve G_3-V_3 is still qualitatively the same as the curve $A(\omega)-\omega$ when $\Gamma_3 \sim \Gamma$. Therefore, the probing lead is not necessarily need to be weakly coupled to the SMT, and the device can still work at $\Gamma_3 \sim \Gamma$. (iii) When Γ_3 is much larger than Γ (e.g. $\Gamma_3 = 4\Gamma$ or more), the side peaks in the conductance G_3 fade away, and the curves

of G_3-V_3 and $A(\omega)-\omega$ have a large discrepancy. Since the properties [including the spectral function $A(\omega)$] of SMT are remarkably influenced when the coupling between the third lead (i.e. exploring terminal) and the SMT is very strong, the differential conductance can no longer exhibit the characteristics of the real spectral function. From Fig.4, it can be concluded that the qualitative agreement between the curves of G_3-V_3 and $A(\omega)-\omega$ is destroyed when $\Gamma_3 > 2(\Gamma_L + \Gamma_R)$.

Now let us consider how temperature influence the relationship between the spectral function and the differential conductance. As displayed in Fig.5a, at low temperature ($T = 0.05\Gamma$) the curve of the spectral function overlaps perfectly with that of the differential conductance, as being discussed before. When temperature is raised to 0.1Γ , although the peaks of the differential conductance are slightly lower (about a few percent) and wider than those of the spectral function, they still agree not only in their positions, but also in the shape of the peaks and the detail structure of the phonon-assisted side peaks (see Fig.5b). With further increasing temperature T , the deviation between the conductance G_3 and the spectral function $A(\omega)$ is more noticeable. When $T = 0.5\Gamma$, the peak heights of the conductance decrease to half of those of the spectral function. In particular, the shapes of the side peaks in the conductance and in the spectral function are clearly in disparity. The shapes of the side peaks of the spectral function are still asymmetric and the change is quite abrupt on one side of the side peak, but the shapes of the side peaks of the differential conductance are Lorentzian and symmetric (see Fig.5c). While the temperature is equal to or larger than Γ , all side peaks of the differential conductance fade away, and the differential conductance is no longer providing any information on the spectral function (see Fig.5d). Therefore, it is feasible only at the low temperature to observe the spectral function by measuring the differential conductance of the third terminal. In the Fig.5, we choose zero bias and the renormalized level $\bar{\epsilon}_0$ located at zero. In fact, all conclusions remain for non-zero bias and any value of $\bar{\epsilon}_0$.

Unlike the coupling strength Γ_3 , the temperature strongly influences the comparability of the curves G_3-V_3 and $A(\omega)-\omega$. When temperature is low enough ($k_B T \ll \Gamma, \hbar\omega_0$), there is a well-defined boundary for the occupied states and empty states in the exploring terminal. With a change of the terminal voltage V_3 , the change of incident electrons concentrate at a very small energy region, thus the differential conductance gives an excellent mapping of the spectral function. On the other hand, this well-defined boundary for the occupied and empty states is destroyed when the temperature $k_B T \sim \Gamma$, so that the conductance G_3 and the spectral function $A(\omega)$ have a large discrepancy. Naturally, if the third lead can be individually fixed at low temperature, then the spectral

function can still be obtained from the differential conductance of the third lead regardless of the temperature in other parts of the system. In fact, the situation with low temperature for the third lead is always comparable with the above discussed low temperature regime. Let us discussed the realizability of the low temperature condition $k_B T \ll \Gamma, \hbar\omega_0$ in the present technology. In an experiment, the characteristic frequency of phonon is about from $5meV$ to $50meV$,^{2,3} and the coupling strength Γ is usually in the order of $100\mu eV$. But the temperature can reach $50mK$ in the present technology. So it should be achievable for the condition $k_B T \ll \Gamma, \hbar\omega_0$. In addition, in experiments the third weakly-coupled lead can be a probing STM tip, and then the coupling strength can be easily controlled by adjusting the distance between the STM tip and the SMT.

At end, we make one more comment. Since we have used the same approximation as in Ref.(¹⁰), the spectral function $A(\omega)$ is completely same as in their work. If to take a different approximation [e.g. as in Ref.(⁹)], the spectral function $A(\omega)$, in particular the shape of the phonon-assisted side peaks, perhaps may vary somewhat. However, the perfect matching for the curves G_3-V_3 and $A(\omega)-\omega$ still maintain as long as at low temperature and weak coupling conditions are met.

V. CONCLUSIONS

In summary, we study the transport behaviors of the three terminal SMT device coupled to a phonon mode. It is found that the intriguing characteristic of the phonon-assisted side peaks in the spectral function versus the energy can be directly observed from the differential conductance versus the voltage of the third weakly-coupled lead. In particular, not only the positions but also the shapes and the detailed structure of the side peaks of the spectral function can be perfectly mapped into the conductance if certain experimental conditions are met. Moreover we determine the conditions for this perfect mapping. The results exhibit that this mapping is excellent at low temperature regardless of the bias and the level of the SMT. The mapping is destroyed at high temperature.

VI. ACKNOWLEDGMENTS

We thank Jianing Zhuang and Haijun Zhang for their helpful discussions. This work is supported by NSF-China under Grant Nos. 90303016, 10474125, and 10525418, US-DOE under Grant No. DE-FG02-04ER46124, and NSF under CCF-052473.

* Electronic address: sunqf@aphy.iphy.ac.cn

¹ H. Park, J. Park, A. K. L. Lim, E. H. Anderson, A. P.

- Alivisatos, and P. L. McEuen, *Nature (London)* **407**, 57 (2000).
- ² B. J. LeRoy, S. G. Lemay, J. Kong, and C. Dekker, *Nature* **432**, 371 (2004).
 - ³ B. J. LeRoy, J. Kong, V. K. Pahlwani, C. Dekker, and S. G. Lemay, *Phys. Rev. B* **72**, 075413 (2005).
 - ⁴ S. Sapmaz, P. Jarillo-Herrero, Y. M. Blanter, C. Dekker, and H. S. J. van der Zant, *Phys. Rev. Lett.* **96**, 026801 (2006).
 - ⁵ N. S. Wingreen, K. W. Jacobsen, and J. W. Wilkins, *Phys. Rev. B* **40**, 11834 (1989).
 - ⁶ M. Keil and H. Schoeller, *Phys. Rev. B* **66**, 155314 (2002).
 - ⁷ David M.-T. Kuo and Y. C. Chang, *Phys. Rev. B* **66**, 085311 (2002).
 - ⁸ J. X. Zhu and A. V. Balatsky, *Phys. Rev. B* **67**, 165326 (2003).
 - ⁹ K. Flensberg, *Phys. Rev. B* **68**, 205323 (2003).
 - ¹⁰ Z. Z. Chen, R. Lu and B. F. Zhu, *Phys. Rev. B* **71**, 165324 (2005).
 - ¹¹ A. Mitra, I. Aleiner and A. J. Millis, *Phys. Rev. B* **69**, 245302 (2004).
 - ¹² Q.-F. Sun and H. Guo, *Phys. Rev. B* **64**, 153306 (2001); E. Lebanon and A. Schiller, *Phys. Rev. B* **65**, 035308 (2002).
 - ¹³ S. De Franceschi, R. Hanson, W. G. van der Wiel, J. M. Elzerman, J. J. Wijkema, T. Fujisawa, S. Tarucha, and L. P. Kouwenhoven, *Phys. Rev. Lett.* **89**, 156801 (2002); R. Leturcq, L. Schmid, K. Ensslin, Y. Meir, D. C. Driscoll, and A. C. Gossard, *Phys. Rev. Lett.* **95**, 126603 (2005).
 - ¹⁴ G. D. Mahan, *Many-Particle Physics*, 3rd ed. (Plenum Press, New York, 2000).
 - ¹⁵ Y. Meir and N. S. Wingreen, *Phys. Rev. Lett.* **68**, 2512 (1992).
 - ¹⁶ A. -P. Jauho, N. S. Wingreen and Y. Meir, *Phys. Rev. B* **50**, 5528 (1994).
 - ¹⁷ H. Huag and A.-P. Jauho, *Quantum Kinetics in Transport and Optics of Semiconductors*, edited by Dr. -Ing. Helmut K. V. Lotsch (Springer-Verlag, Berlin Heidelberg, 1996).
 - ¹⁸ Here we assume that the isolated phonon system is in equilibrium, thus, this temperature is the same as that for the electronic part. In fact, even if the phonon and electron temperatures are different, namely the electron and the phonon systems are not in equilibrium, which may occurs in a real experimental under a bias, the main results, *i.e.*, the curve $A(\omega)-\omega$ can map into the curve G_3-V_3 , still remains, as soon as the electron temperature is sufficiently low.

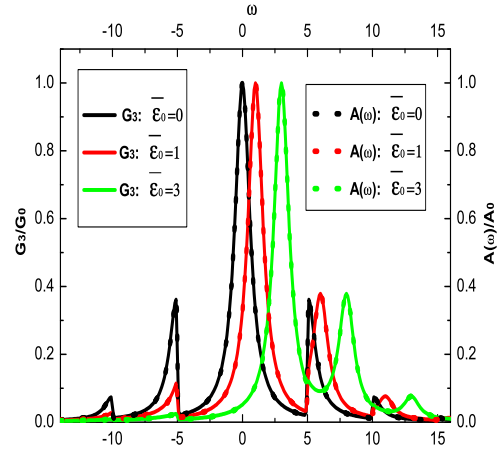


FIG. 2: (Color online) The dimensionless spectral function $A(\omega)/A_0$ vs. the energy ω at $\Gamma_3 = 0$ and the dimensionless differential conductance G_3/G_0 of the third lead vs. the voltage V_3 at $\Gamma_3 = 0.01$ for different ϵ_0 . Other parameters are taken as: $u_L = u_R = 0$, $\omega_0 = 5$, $T = 0.02$, and $\lambda = 3$. The unites A_0 and G_0 are equal to $2/\Gamma$ and $(2e^2/h)(\Gamma_3/\Gamma)$ respectively. Notice that the three dotted curves almost overlap perfectly with the three solid curves so that they almost cannot be seen in the figure.

FIG. 1: Schematic diagram of a SMT coupled to three leads with tunnelling strength Γ_α and the electron in the SMT is also coupled to a single-phonon mode. A gate electrode is capacitively attached to the SMT to tune the energy level of SMT.

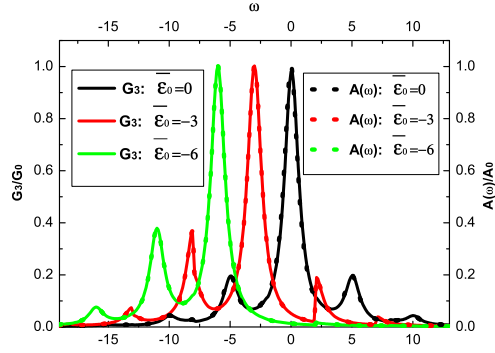


FIG. 3: (Color online) The dimensionless spectral function $A(\omega)/A_0$ vs. the energy ω at $\Gamma_3 = 0$ and the dimensionless differential conductance G_3/G_0 of the third lead vs. the voltage V_3 at $\Gamma_3 = 0.01$ for different $\bar{\epsilon}_0$, with $u_L = -u_R = 3$. The other parameters are same with Fig.2. Notice that the three dotted curves almost overlap perfectly with the three solid curves so that they almost cannot be seen in the figure.

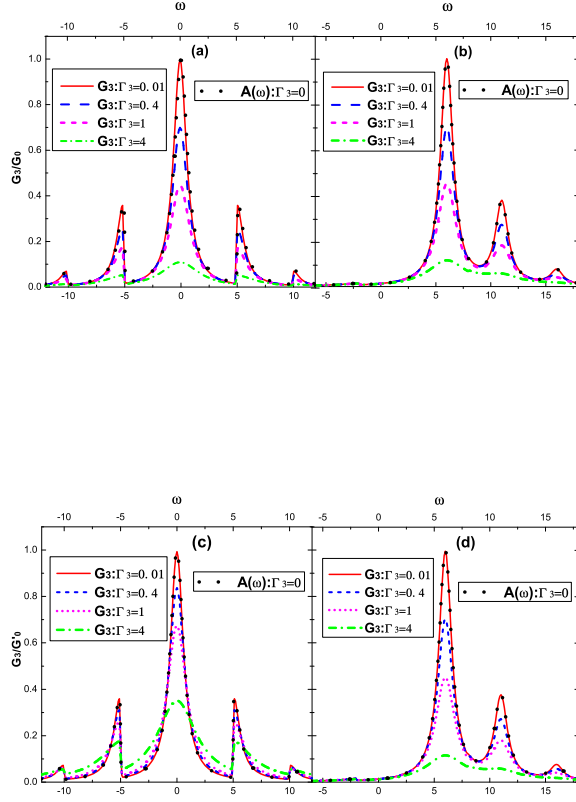


FIG. 4: (Color online) The dimensionless spectral function $A(\omega)/A_0$ vs. the energy ω and the dimensionless differential conductance G_3 of the third lead vs. the voltage V_3 for different coupling strengths Γ_3 . The parameters are taken as: $\omega_0 = 5$, $T = 0.02$, and $\lambda = 3$. (a,c) and (b,d) are corresponding to $u_L = u_R = 0$ and $\bar{\varepsilon}_0 = 0$, and $u_L = -u_R = 3$ and $\bar{\varepsilon}_0 = 6$, respectively. The units $A_0 = 2/\Gamma$, $G_0 = (2e^2/h)(\Gamma_3/\Gamma)$, and G'_0 is determined by the equation $\int \frac{dV_3}{2\pi} \frac{G_3(V_3)}{G'_0} = \int \frac{d\omega}{2\pi} \frac{A(\omega)}{A_0}$.

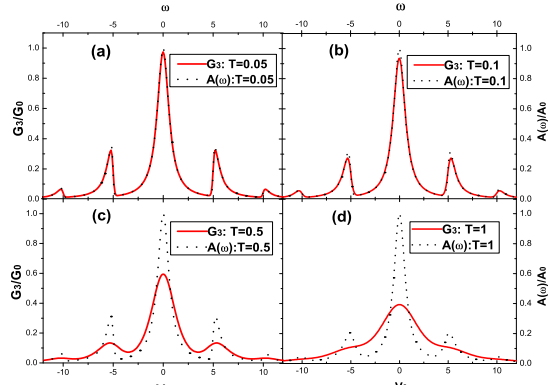


FIG. 5: (Color online) The dimensionless spectral function $A(\omega)/A_0$ vs. the energy ω at $\Gamma_3 = 0$ and the dimensionless differential conductance G_3/G_0 of the third lead vs. the voltage V_3 at $\Gamma_3 = 0.01$ for different temperatures. The other parameters are $u_L = u_R = 0$, $\omega_0 = 5$, $\bar{\epsilon}_0 = 0$, and $\lambda = 3$. The unites $A_0 = 2/\Gamma$ and $G_0 = (2e^2/\hbar)(\Gamma_3/\Gamma)$.

